Applied Physics Letters

Extension of the two-layer model to heat transfer coefficient predictions of nanoporous Si thin films

Cite as: Appl. Phys. Lett. **121**, 012201 (2022); https://doi.org/10.1063/5.0099312
Submitted: 16 May 2022 • Accepted: 17 June 2022 • Published Online: 06 July 2022

Sien Wang, Qiyu Chen and Qing Hao

AIP Publishing

Applied Physics Letters ARTICLE scitation.org/journal/apl

Extension of the two-layer model to heat transfer coefficient predictions of nanoporous Si thin films

Cite as: Appl. Phys. Lett. **121**, 012201 (2022); doi: 10.1063/5.0099312
Submitted: 16 May 2022 · Accepted: 17 June 2022 ·
Published Online: 6 July 2022

Sien Wang, Qiyu Chen, and Qing Hao[a]

AFFILIATIONS

Department of Aerospace and Mechanical Engineering, University of Arizona, Tucson, Arizona 85721-0119, USA

Note: This paper is part of the APL Special Collection on Thermal Radiation at the Nanoscale and Applications.
[a]**Author to whom correspondence should be addressed:** qinghao@email.arizona.edu

ABSTRACT

Heat exchange between a solid material and the gas environment is critical for the heat dissipation of miniature electronic devices. In this aspect, existing experimental studies focus on non-porous structures such as solid thin films, nanotubes, and wires. In this work, the proposed two-layer model for the heat transfer coefficient (HTC) between a solid sample and the surrounding air is extended to 70-nm-thick nanoporous Si thin films that are patterned with periodic rectangular nanopores having feature sizes of 100–400 nm. The HTC values are extracted using the 3ω method based on AC self-heating of a suspended sample with better accuracy than steady-state measurements in some studies. The dominance of air conduction in the measured HTCs is confirmed by comparing measurements with varied sample orientations. The two-layer model, developed for nanotubes, is still found to be accurate when the nanoporous film is simply treated as a solid film in the HTC evaluation along with the radiative mean beam length as the characteristic length of the nanoporous film. This finding indicates the potential of increasing HTC by introducing ultra-fine nanoporous patterns, as guided by the two-layer model.

Thermal transport within various micro- to nano-structures has been intensively studied for applications in thermal management,[1] thermoelectrics,[2,3] and electronic devices.[4] Although thermal conductivity measurements are usually carried out in high vacuum,[5] the real applications of these structures are in ambient conditions, where the heat loss to the surrounding air becomes critical due to its ultrahigh surface-to-volume ratios. This issue is even more critical when the micro- and nano-structures are suspended as the active device component, e.g., microelectromechanical (MEMS) systems,[6] sensors,[7,8] and field emitters.[9] A better understanding of the solid–gas energy exchange at small scales is important for both fundamental studies and practical applications. Currently, it is still challenging to accurately predict the corresponding heat transfer coefficient (HTC) at the solid–gas interface. Although the HTC is often attributed to natural convection for macro-scale samples, the dominant heat transfer mechanism is considered to be gas conduction for nano- to micro-structures.[10] With a short length scale associated with the heat conduction of the gas, the thermal conductance of the gas can be orders of magnitude higher than the natural convection HTC when the scale is below a few micrometers.[11]

The HTC modeling at a gas–solid interface at small scales has been treated differently in the literature. For a suspended thin film, the HTC (h) was treated as pure heat conduction by the surrounding air. This value h depended on the air thermal conductivity, the heat-conduction shape factor, and sample geometry.[10] Another report evaluated the HTC of a microbeam by considering the air conduction from a specimen to the nearest solid surface and the competition between in-sample heat conduction and the surface convection.[12] In more advanced modeling, a two-layer heat transfer model was developed to predict the HTC (see the supplementary material for details).[11,13–16] Fuchs first proposed this model for heat transfer between the gas environment and isolated particles at sub-microscales.[14,15] The model was improved by Klein *et al.*[13] and extended to cylindrical carbon nanotubes (CNTs) by Wang *et al.*[11,16] The inner non-continuum layer around the solid surface has thickness comparable to the mean free path (MFP) of gas molecules. Inside this layer, the solid–gas molecule interaction and intermolecular collision are considered to evaluate the net heat flux from the solid surface. In the outer continuum layer, heat conduction is assumed to be the major heat transfer mode, and Fourier's law analysis is employed. For other nano-structures such as solid or nanoporous thin films, the two-layer model should be modified to account for more complicated interactions between gas molecules and nano-structured surfaces.

Different techniques have been employed for HTC measurements, including the 3ω method,[10,17,18] steady-state laser/Joule heating

and Raman temperature reading,[11,19–21] Joule heating and infrared thermal microscopy,[12] the thermal response of a microcantilever under sinusoidal heating,[22] laser thermography based on the observed one-dimensional domain structure,[23] and the "hot wire" method based on the sample self-heating.[24–27] The size of measured samples expands a wide range from a few nanometers to tens of micrometers with more studies focusing on wires. The reported HTC is $\sim 10^2$ W/m^2 K for conventional metal wires with a diameter from 10 to 100 μm.[18,25,26] In the sub-micrometer regime, extremely high HTCs with magnitudes from 10^3 to 10^4 W/m^2 K were observed for nanowires (NWs) and carbon nanotubes (CNTs).[11,21,23] Among those, a 1.47-nm-diameter CNT exhibited an HTC of 0.9×10^5 W/m^2 K in air.[11] The value is approaching the limit of $h_{max} = 5nuk_B/8 = 1.1 \times 10^5$ W/m^2 K as predicted by the classical gas kinetic theory.[28] Here, k_B is the Boltzmann constant, n is the molecular density, and u is the root mean square (RMS) velocity. In estimation, $u = \sqrt{3k_BT/m}$, where m is the gas-molecule mass and T is the absolute temperature. Similarly, the two-layer model predicts $h_{max} = 1.08 \times 10^5$ W/m^2 K.[11] For suspended samples fabricated from thin films,[10,12,17] the reported HTCs are at least two orders of magnitude higher than that of the natural convection at the macroscale. Experimental studies were also extended to arrays of CNTs or NWs. Enhanced heat dissipation to the ambient was found in vertically aligned CNTs due to the increased surface area added by individual CNTs.[29,30] The influence of the nano-structure gap was further reported for a row of parallel nickel microwires.[27] With the same self-heating of microwires, the temperature rise ΔT of the microwires started to increase when the gap between adjacent microwires became less than double the MFP of an ambient medium. For systematic studies, periodic nanoporous thin films widely studied for thermoelectrics[31–36] can be used as the test bed. In the geometry, such nanoporous thin films can be viewed as two-dimensional networks of NWs. Compared with individual NWs, nanoporous thin films can transport significantly more heat. To achieve a high surface-to-volume ratio, ultra-fine nanoporous patterns can be exactly defined across such thin films with electron beam lithography (EBL). A wide range of nano-structure sizes can be fabricated for fundamental studies.

In this work, the HTCs of representative nanoporous 70-nm-thick Si films were measured using the 3ω method.[37] The method was adopted to separately measure the intrinsic thermal conductivity of a thin film and its HTC with the surrounding air. Different rectangular nanopores (i.e., nanoslots) were patterned to investigate the impact of the surface-to-volume ratio on the HTC. The smallest feature size was around 100–200 nm to represent the device resolution that can be easily achieved by techniques such as extreme UV lithography[38] or nanosphere lithography[39] for mass production. Our measurement result agrees well with the theoretical prediction based on the two-layer heat transfer model that is developed for tubes and wires.[11] By etching smaller and denser nanopores, the HTC could be further increased. The probability of the gas molecule collision with the solid surface can be enhanced with higher surface-to-volume ratio. The predicted 1.08×10^5 W/m^2 K peak h value[11] can be potentially approached with ultra-fine nanoporous patterns for heat dissipation purposes.

Suspended silicon thin films with rectangular nanopores were prepared for thermal measurements. The device was fabricated from a silicon-on-insulator (SOI) wafer with a 70-nm-thick device layer and a 2-μm-thick buried oxide (BOX) layer. Rectangular nanopores were defined with EBL and drilled with reactive ion etching (RIE). The device was then suspended by removing the underneath BOX with diluted hydrofluoric (HF) acid. Due to the low intrinsic electrical conductivity of the undoped Si, a metal layer consisting of Cr (20 nm) and then Pt (40 nm) was deposited on top of the device with electron beam evaporation. This layer was used as both the heater and electrical resistance thermometer in thermal measurements. Figure 1 shows the scanning electron microscopy (SEM) image of a suspended device with four electrical probes. The measured region is 20 μm in length and 2 μm in width. Compared with other measurement techniques, the integrated device here eliminates the sample-device thermal contact issue that becomes critical for similar measurements.[34,35,40] It is now acknowledged that an integrated device fabricated from the same thin film can be an ideal choice for such thermal studies.[41–43]

In measurements, an AC heating current of an angular frequency ω was passed through the metal coating, and the 3ω voltage ($V_{3\omega}$) across the sample was measured with a lock-in amplifier. For in-air measurements, the root mean square (RMS) value of $V_{3\omega}$ is derived by Lu *et al.* as[37]

$$V_{3\omega} \approx \frac{4I^3LR(dR/dT)}{\pi^4 A_c k_{ap}\sqrt{1+(2\omega\gamma_{ap})^2}}. \quad (1)$$

Here, the apparent thermal conductivity (k_{ap}) and time constant (γ_{ap}) can be extracted by fitting the $V_{3\omega}(\omega)$ curve with Eq. (1). In particular, the value k_{ap} is mostly determined by the $V_{3\omega}$ value or the slope $dV_{3\omega}/d(I^3)$ at the limit $\omega\gamma_{ap} \to 0$. Other parameters are RMS current I, sample length L, electrical resistance R, and cross-sectional area A_c. In the derivation, k_{ap} and γ_{ap} are given as

$$k_{ap} = (1 + \mathcal{H}\gamma)k, \quad (2a)$$

$$\gamma_{ap} = \gamma/(1 + \mathcal{H}\gamma). \quad (2b)$$

Considering air conduction instead of radiation loss in the original work by Lu *et al.*, $\mathcal{H} = A_s h/\rho V C_p$ can be derived, where A_s is the surface area of the sample sidewall, h is the HTC, ρ is the density, V is the volume of the sample, and C_p is the heat capacity.

For high-vacuum measurements, Eq. (1) is simplified with $\mathcal{H} = 0$, $k_{ap} = k$, and $\gamma_{ap} = \gamma$, which leads to the original equation given by Lu *et al.*[37] In Eq. (2), k and γ can be first fitted from the

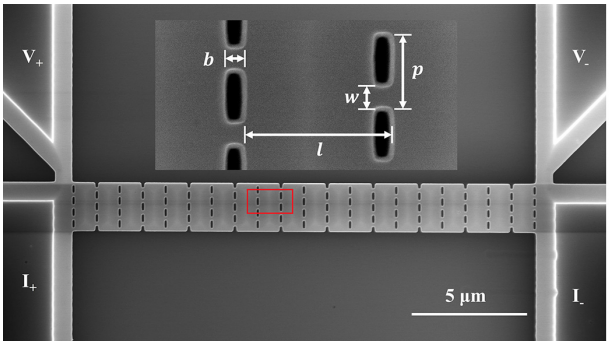

FIG. 1. SEM image of a typical four-probe device with the suspended nanoporous Si thin film in the middle. The inset shows the detailed structure with major geometry parameters defined.

TABLE I. Room-temperature thermal properties measured for different samples. The definition of geometry factors (pitches *l* and *p*, depth *b*, and neck width *w*) is given in Fig. 1. Samples 2, 3, and 6 have offset nanopores as shown in Fig. 1, whereas samples 4 and 5 have aligned nanopores.

Sample index	*l* (nm)	*p* (nm)	*b* (nm)	*w* (nm)	*k* (W/m K)	Solid *C* (kJ/m^3 K)
1		Solid film			58.28	2188.4
2	1000	500	120	160	18.85	2095.9
3	1000	500	200	80	13.36	2100.9
4	500	500	200	80	7.83	2312.8
5	250	500	100	160	9.85	2322.7
6	250	500	100	160	6.96	2267.9

$V_{3\omega}(\omega)$ curve obtained from in-vacuum measurements. Again, the value k is mostly determined by the $V_{3\omega}$ value at the limit $\omega\gamma \to 0$. The h value can then be calculated with Eq. (2a) as

$$h = \left(\frac{k_{ap}}{k} - 1\right)\frac{\rho C_p}{\gamma}\frac{V}{A_s}. \tag{3}$$

The employed 3ω technique can yield k and h for the same sample. Similar measurements can be found in previous 3ω measurements by Nguyen *et al.*[17] and steady-state thermal measurements using a Joule-heating-Raman-mapping technique by Li *et al.*[20] Here, Li *et al.* further measured the specific heat of CNTs with the transient electro-thermal technique. In this work, the volumetric specific heat C of the metal-coated film can also be computed as $C = \pi^2 k\gamma/L^2$,[37] which was well calibrated in our previous studies.[41]

The k and C values for all measured samples are listed in Table I. For a solid film, the room-temperature in-plane $k \approx 58$ W/m K was close to the computed $k \approx 64$ W/m K.[44] The metal-layer contribution was subtracted with the calibrated Lorenz number for the metal coating and the measured electrical conductance of this metal layer.[41] It should be noted that the Lorenz number may largely vary among nano- and micro-structures.[45–47] In this work, the metal-layer thickness and its deposition condition exactly followed those in the previous work[41] so that the pre-calibrated temperature-dependent Lorenz number was still accurate. Nevertheless, the Lorenz number was not required in the calculation of h in Eq. (3), as the effective in-plane k_{ap} and k of the whole metal-coated film were used. In calibrations with a solid film at 77–300 K,[48] the divergence was within 2.2% between three samples measured with: (1) 3ω measurements for a suspended beam;[41] or (2) a T-junction device with a long heating/sensing beam and its perpendicular short beam as "the sample."[49–51] Corrections for the porosity φ should be considered to compare different samples. The solid specific heat C, as measured specific heat divided by $(1-\varphi)$, was consistent with predicted solid $C = 2194.4$ kJ/m^3 K using bulk C value for different layers of a coated thin film. Some of the <6% divergence here is attributed to the accuracy in the estimated φ.[41] The above mentioned comparisons ensure highly accurate measurements for the studied nanoporous films.

The detailed measurement result of a solid film is presented in Fig. 2. Following Eq. (1), linear fittings for $V_{3\omega} \sim I^3$ at a fixed ω all exhibit $R^2 > 0.99995$ [Fig. 2(a)]. The k_{ap}/k ratio in Eq. (3) can be obtained from the ratio between $dV_{3\omega}/d(I^3)$ slopes at a fixed low ω. The low-frequency k_{ap}/k ratio is very close to 1.5113 obtained by extracting the exact value of k and k_{ap} from the full $V_{3\omega} - \omega$ curve fitting in Fig. 2(b). The $V_{3\omega}(\omega)$ response of the sample in air and a high vacuum are compared in Fig. 2(b). For the same heating current, $|V_{3\omega}|$ is much lower for the in-air measurements due to the significant heat loss by the air conduction. Similar to the work by Hu *et al.*,[10] the in-air measurement was further repeated with different sample orientations to check the impact of the natural convection. Variation of less than 1% was found in Fig. 2(b), indicating negligible influence of the natural convection.

For the nanoporous film, the HTCs can be defined in two ways based on the effective surface area for heat exchange. In Eq. (3), an effective HTC (h_{eff}) can be calculated when A_s (i.e., $20 \times 2\ \mu$m^2 for top/bottom surfaces) for the corresponding solid film is used, i.e., no correction for the porosity. In real applications, using such a "nominal" surface area allows direct comparison between different devices for heat loss estimation. The true HTC h_{true} can be computed when A_s is replaced by the true surface area $A_{s,true}$, including the sidewall surface area of nanopores. In this treatment, the pore sidewalls are treated equally as the top/bottom film surfaces though the latter one may have more efficient energy exchange with the gas molecules. It can be expected that h_{true} should decrease when the pore sidewalls account for a larger percentage of the total surface area, particularly for high-aspect-ratio nanopores. For a very long and narrow rectangular nanopore with depth b (Fig. 1 inset), it can be proven that $A_{s,true}$ would increase by adding nanopores with b smaller than the film thickness. Similar discussions can be found for cylindrical pores. The associated surface energy variation determines whether a nanopore would shrink or expand under high-temperature annealing.[52,53]

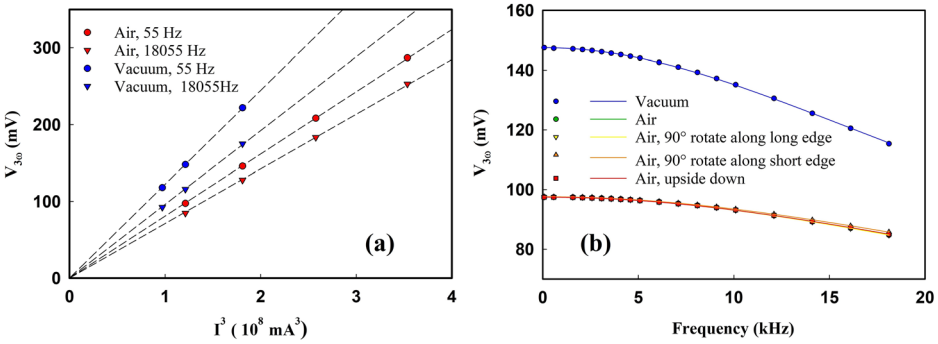

FIG. 2. Measurement results of a solid film. (a) Linear relationship between $V_{3\omega}$ and I^3. (b) Comparison of the $V_{3\omega}$ signals between in-vacuum and in-air measurements with the same AC heating current of 0.7 mA in amplitude. The in-air measurement was carried out with different sample orientations.

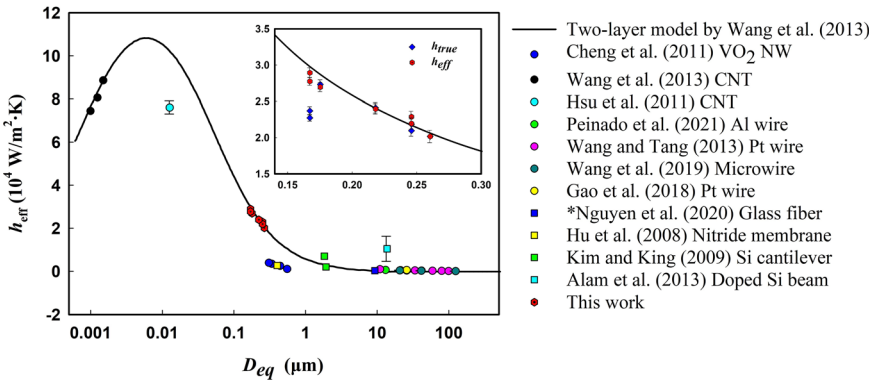

FIG. 3. Comparison between measured HTCs of various micro- to nano-structures and the two-layer model by Wang *et al.*[11] As one exception, measurements by Nguyen *et al.*[17] are in nitrogen instead of the air. Inset shows the detailed comparison for samples measured in this work, where blue symbols are added for the corresponding h_{true} values.

Our experimental results are further compared with the two-layer model[11] and existing measurements (Fig. 3). These measurements include VO_2 NWs by Cheng *et al.*,[23] CNTs by Wang *et al.*[11] and by Hsu *et al.*,[21] Al wires by Peinado *et al.*,[26] Pt wires by Wang and Tang[18] and Gao *et al.*,[25] various microwires by Wang *et al.*,[24] glass fibers by Nguyen *et al.*,[17] nitride membranes by Hu *et al.*,[10] Si cantilevers by Kim and King,[22] and doped Si beams by Alam *et al.*[12] In one study, air conduction from a suspended film to the experimental chamber is considered.[17] However, the current 2-μm gap as the BOX thickness is much larger than the air-molecule MFPs (~68 nm at room temperature[54]) so that the two-layer model is still valid. To unify the data of different sample geometries for the two-layer model, an equivalent diameter, $D_{eq} = 4V_{solid}/A_{s,true}$, is used as the characteristic length. Here, V_{solid} is the solid volume of the structure. This D_{eq} is simply the radiative mean beam length of a structure.[55–57] It should be pointed out that the h_{eff} for the nanoporous thin film is used here. Divergence between the two-layer model and h_{true} (blue symbols) is further shown in the inset.

Attention should be given to the use of the nominal surface area for the heat-exchanging surface area. For high-aspect-ratio and narrow nanopores, the chance for a gas molecule to directly pass through the nanopore is very limited, particularly when the film thickness is also larger than the gas-molecule MFP. Most gas molecules moving into the nanopores will be captured by the nanopore sidewall and eventually scattered out of the nanopores. The effective area to "receive" incident gas molecules from the surrounding should be the "opening" regions on the top/bottom surfaces of the thin film, instead of the sidewall surface area of the nanopores [Fig. 4(a)]. Compared with gas molecules directly reflected by the top/bottom film surfaces, these gas molecules are simply trapped in the nanopore for some time and then released to the surrounding. In this aspect, the number of gas molecules traveling into nanopores per unit time, known as the molecular impact flux[11] into nanopores, is weakly affected by the nanopore size and film thickness. However, the exact nanoporous pattern and film thickness can still influence D_{eq} used in the derived $h(D_{eq})$ expression (see the supplementary material).[11,16] In physics, D_{eq} and, thus, the Knudsen Number Λ/D_{eq} determine the relative importance between the intermolecular collisions and solid–gas scattering. Because the non-continuum layer has a fixed thickness comparable to Λ, the D_{eq} also affects the geometry of the continuum and non-continuum layers and the corresponding heat-conduction process. Following this, D_{eq} around 10 nm is required to approach the h_{max} value in Fig. 3. A square period with a square pore in the middle is considered to achieve this D_{eq} value with $p = l$ and porosity $\varphi \equiv 25\%$ [Fig. 4(b)]. With $p = l = 5$ nm and a film thickness $t = 70$ nm, D_{eq} around 7.1 nm can be achieved.

In summary, a modified 3ω method is used to measure the HTC of nanoporous Si thin films with rectangular pores. Based on the nominal surface area, the h_{eff} values for such nanoporous structures still follow the predictions by the two-layer model developed for CNTs. The radiative mean beam length is used to define the equivalent diameter D_{eq} in the modeling. This important modification allows us to predict the HTC of suspended structures with arbitrary shapes and porosity, which is verified with the experimental results from this

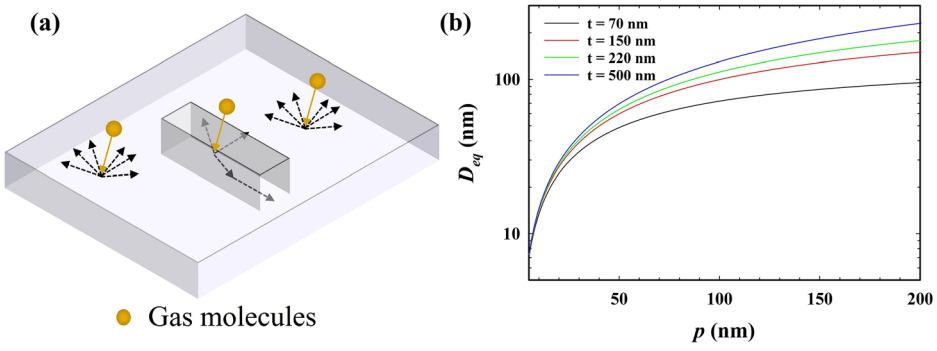

FIG. 4. (a) Gas molecules incident onto a nanoporous film. The number of molecules trapped by a nanopore is mainly dependent on the opening area on the top/bottom surfaces of the thin film. These gas molecules will eventually leave the nanopore after being scattered by the sidewall. (b) D_{eq} as a function of the pitch $p = l$ and film thickness t. The porosity is fixed at $\varphi \equiv 25\%$.

work and previous studies. It should be noted that qualitative models for HTCs have been proposed for suspended solid thin films[10] and rectangular beams,[12] mainly based on air conduction from the sample to the surrounding solid surfaces. The non-continuum layer is not considered in such simplified models. In contrast, the two-layer model can provide accurate predictions when the suspended sample is away from other surfaces (e.g., its underlying substrate) by a distance much longer than the gas-molecule MFPs. For nanoporous thin films, the solid–gas interaction is enhanced due to the increased surface-to-volume ratio, leading to a smaller D_{eq}. Attention should be paid to the less effective energy exchange on the nanopore sidewall, especially for a high aspect ratio of such nanopores. When such nanoporous films are used as fins, the film thickness and nanoporous patterns should be optimized to have both strong surface cooling and sufficient in-plane heat conduction for heat dissipation. Aside from its applications in thermoelectric cooling of a device,[36] a nanoporous thin film can be easily integrated into electronic devices as fins. Fundamentally, solid–gas energy exchange for more complicated three-dimensional nanoporous structures should also be studied to better understand this critical problem. Some studies may be further carried out on the pressure dependence of h_{eff}.[17,23,25,27]

See the supplementary material for the derivation of the two-layer heat transfer model.

The author acknowledges the support from the National Science Foundation CAREER Award (Grant No. CBET-1651840). SEM analyses were performed at the Kuiper Materials Imaging and Characterization facility at the University of Arizona.

AUTHOR DECLARATIONS

Conflict of Interest

The authors have no conflicts to disclose.

Author Contributions

Sien Wang: Conceptualization (equal); Formal analysis (equal); Investigation (equal); Methodology (equal); Visualization (equal); Writing – original draft (equal). **Qiyu Chen:** Visualization (equal). **Qing Hao:** Conceptualization (equal); Formal analysis (equal); Funding acquisition (equal); Methodology (equal); Project administration (equal); Writing – review and editing (equal).

DATA AVAILABILITY

The data that support the findings of this study are available from the corresponding author upon reasonable request.

REFERENCES

[1]Y. Xiao, Q. Chen, and Q. Hao, Mater. Today Phys. **21**, 100477 (2021).
[2]Q.-Y. Li, Q. Hao, T. Zhu, M. Zebarjadi, and K. Takahashi, Eng. Sci. **13**, 24–50 (2020).
[3]G. Pennelli, Beilstein J. Nanotechnol. **5**, 1268–1284 (2014).
[4]D. G. Cahill, P. V. Braun, G. Chen, D. R. Clarke, S. Fan, K. E. Goodson, P. Keblinski, W. P. King, G. D. Mahan, and A. Majumdar, Appl. Phys. Rev. **1**(1), 011305 (2014).
[5]K. Hippalgaonkar, J. Hun Seol, D. Xu, and D. Li, in *Thermal Transport in Carbon-Based Nanomaterials*, edited by G. Zhang (Elsevier, 2017), pp. 319–357.
[6]Y. Zhu and T.-H. Chang, J. Micromech. Microeng. **25**(9), 093001 (2015).
[7]C. Yu, Q. Hao, S. Saha, L. Shi, X. Kong, and Z. L. Wang, Appl. Phys. Lett. **86**(6), 063101 (2005).
[8]M. C. Lemme, S. Wagner, K. Lee, X. Fan, G. J. Verbiest, S. Wittmann, S. Lukas, R. J. Dolleman, F. Niklaus, H. S. J. van der Zant, G. S. Duesberg, and P. G. Steeneken, Research **2020**, 8748602.
[9]H. D. Nguyen, J. S. Kang, M. Li, and Y. Hu, Nanoscale **11**(7), 3129–3137 (2019).
[10]X. J. Hu, A. Jain, and K. E. Goodson, Int. J. Therm. Sci. **47**(7), 820–824 (2008).
[11]H.-D. Wang, J.-H. Liu, X. Zhang, T.-Y. Li, R.-F. Zhang, and F. Wei, J. Nanomater. **2013**, 181543.
[12]M. T. Alam, A. P. Raghu, M. A. Haque, C. Muratore, and A. A. Voevodin, Int. J. Therm. Sci. **73**, 1–7 (2013).
[13]H. H. Klein, J. Karni, R. Ben-Zvi, and R. Bertocchi, Sol. Energy **81**(10), 1227–1239 (2007).
[14]N. Fuchs, Geofis. Pura Appl. **56**(1), 185–193 (1963).
[15]N. A. Fuchs, R. Daisley, M. Fuchs, C. Davies, and M. Straumanis, Phys. Today **18**(4), 73 (1965).
[16]H.-D. Wang, J.-H. Liu, Z.-Y. Guo, X. Zhang, R.-F. Zhang, F. Wei, and T.-Y. Li, Nanoscale Microscale Thermophys. Eng. **17**(4), 349–365 (2013).
[17]T. D. Nguyen, J. Richard, J. Doumouro, Y. De Wilde, and O. Bourgeois, J. Heat Transfer **142**(10), 101701 (2020).
[18]Z. L. Wang and D. W. Tang, Int. J. Therm. Sci. **64**, 145–151 (2013).
[19]Q.-Y. Li and X. Zhang, Thermochim. Acta **581**, 26–31 (2014).
[20]M. Li, C. Li, J. Wang, X. Xiao, and Y. Yue, Appl. Phys. Lett. **106**(25), 253108 (2015).
[21]I. K. Hsu, M. T. Pettes, M. Aykol, C.-C. Chang, W.-H. Hung, J. Theiss, L. Shi, and S. B. Cronin, J. Appl. Phys. **110**(4), 044328 (2011).
[22]K. J. Kim and W. P. King, Appl. Therm. Eng. **29**(8), 1631–1641 (2009).
[23]C. Cheng, W. Fan, J. Cao, S.-G. Ryu, J. Ji, C. P. Grigoropoulos, and J. Wu, ACS Nano **5**(12), 10102–10107 (2011).
[24]X. Wang, R. Guo, Q. Jian, G. Peng, Y. Yue, and N. Yang, ES Mater. Manuf. **5**, 65–71 (2019).
[25]J. Gao, D. Xie, Y. Xiong, and Y. Yue, Appl. Phys. Express **11**(6), 066601 (2018).
[26]L. Peinado, V. Muntean, and I. Pérez-Grande, Exp. Therm. Fluid Sci. **122**, 110295 (2021).
[27]M.-H. Seo, J.-H. Park, K.-W. Choi, M.-S. Jo, and J.-B. Yoon, Appl. Phys. Lett. **115**(13), 131901 (2019).
[28]J. E. A. John, *Gas Dynamics* (Allyn and Bacon, Boston, 1933).
[29]Y. Cohen, S. K. Reddy, Y. Ben-Shimon, and A. Ya'akobovitz, Nanotechnology **30**(50), 505705 (2019).
[30]C. Silvestri, M. Riccio, R. H. Poelma, A. Jovic, B. Morana, S. Vollebregt, A. Irace, G. Q. Zhang, and P. M. Sarro, Small **14**(20), 1800614 (2018).
[31]Y. Xiao and Q. Hao, Int. J. Heat Mass Transfer **170**, 120944 (2021).
[32]R. Anufriev, J. Ordonez-Miranda, and M. Nomura, Phys. Rev. B **101**(11), 115301 (2020).
[33]J. Lee, W. Lee, G. Wehmeyer, S. Dhuey, D. L. Olynick, S. Cabrini, C. Dames, J. J. Urban, and P. Yang, Nat. Commun. **8**, 14054–14054 (2017).
[34]J. Tang, H.-T. Wang, D. H. Lee, M. Fardy, Z. Huo, T. P. Russell, and P. Yang, Nano Lett. **10**(10), 4279–4283 (2010).
[35]J.-K. Yu, S. Mitrovic, D. Tham, J. Varghese, and J. R. Heath, Nat. Nanotechnol. **5**(10), 718–721 (2010).
[36]Y. Xiao, Q. Chen, D. Ma, N. Yang, and Q. Hao, ES Mater. Manuf. **5**, 2–18 (2019).
[37]L. Lu, W. Yi, and D. L. Zhang, Rev. Sci. Instrum. **72**(7), 2996–3003 (2001).
[38]N. Fu, Y. Liu, X. Ma, and Z. Chen, J. Microelectron. Manuf. **2**(2), 19020202 (2019).
[39]P. Colson, C. Henrist, and R. Cloots, J. Nanomater. **2013**, 948510.
[40]S. Alaie, D. F. Goettler, M. Su, Z. C. Leseman, C. M. Reinke, and I. El-Kady, Nat. Commun. **6**, 7228 (2015).
[41]Q. Hao, D. Xu, H. Zhao, Y. Xiao, and F. J. Medina, Sci. Rep. **8**(1), 9056 (2018).
[42]J. Lim, H.-T. Wang, J. Tang, S. C. Andrews, H. So, J. Lee, D. H. Lee, T. P. Russell, and P. Yang, ACS Nano **10**(1), 124–132 (2016).
[43]A. M. Marconnet, T. Kodama, M. Asheghi, and K. E. Goodson, Nanoscale Microscale Thermophys. Eng. **16**(4), 199–219 (2012).
[44]C. Jeong, S. Datta, and M. Lundstrom, J. Appl. Phys. **111**(9), 093708 (2012).
[45]Y. Hu, S. Li, and H. Bao, Phys. Rev. B **103**(10), 104301 (2021).

[46]Y. Zhao, M. L. Fitzgerald, Y. Tao, Z. Pan, G. Sauti, D. Xu, Y.-Q. Xu, and D. Li, Nano Lett. **20**(10), 7389–7396 (2020).
[47]S. J. Mason, D. J. Wesenberg, A. Hojem, M. Manno, C. Leighton, and B. L. Zink, Phys. Rev. Mater. **4**(6), 065003 (2020).
[48]Y. Xiao, D. Xu, F. J. Medina, S. Wang, and Q. Hao, Mater. Today Phys. **12**, 100179 (2020).
[49]C. Dames, S. Chen, C. T. Harris, J. Y. Huang, Z. F. Ren, M. S. Dresselhaus, and G. Chen, Rev. Sci. Instrum. **78**(10), 104903–104913 (2007).
[50]W. Jang, W. Bao, L. Jing, C. Lau, and C. Dames, Appl. Phys. Lett. **103**(13), 133102 (2013).
[51]M. Fujii, X. Zhang, H. Xie, H. Ago, K. Takahashi, T. Ikuta, H. Abe, and T. Shimizu, Phys. Rev. Lett. **95**(6), 065502 (2005).
[52]A. Storm, J. Chen, X. Ling, H. Zandbergen, and C. Dekker, Nat. Mater. **2**(8), 537–540 (2003).
[53]Q. Hao, Y. Xiao, and F. J. Medina, ES Mater. Manuf. **6**, 24–27 (2019).
[54]S. G. Jennings, J. Aerosol Sci. **19**(2), 159–166 (1988).
[55]J. R. Howell, M. P. Menguc, and R. Siegel, *Thermal Radiation Heat Transfer* (CRC Press, 2010).
[56]Q. Hao, Y. Xiao, and H. Zhao, J. Appl. Phys. **120**(6), 065101 (2016).
[57]Q. Hao, Y. Xiao, and H. Zhao, Appl. Therm. Eng. **111**, 1409–1416 (2017).